



# Facile in situ synthesis of graphitic carbon nitride (g-C<sub>3</sub>N<sub>4</sub>)-N-TiO<sub>2</sub> heterojunction as an efficient photocatalyst for the selective photoreduction of CO<sub>2</sub> to CO

Sheng Zhou, Ying Liu, Jianmei Li, Yajun Wang, Guiyuan Jiang<sup>\*\*</sup>, Zhen Zhao<sup>\*</sup>, Daxi Wang, Aijun Duan, Jian Liu, Yuechang Wei

State Key Laboratory of Heavy Oil Processing, China University of Petroleum Beijing, Beijing 102249, People's Republic of China

## ARTICLE INFO

### Article history:

Received 25 December 2013  
Received in revised form 9 March 2014  
Accepted 19 March 2014  
Available online 28 March 2014

### Keywords:

Photocatalysis  
CO<sub>2</sub> reduction  
Nitrogen-doped TiO<sub>2</sub>  
Graphitic carbon nitride  
In situ synthesis

## ABSTRACT

A series of composites of graphitic carbon nitride and in situ nitrogen-doped titanium dioxide (g-C<sub>3</sub>N<sub>4</sub>-N-TiO<sub>2</sub>) were prepared by a simple pyrolysis process of urea and Ti(OH)<sub>4</sub>. The obtained products were characterized by means of X-ray diffraction, FT-IR transmission spectroscopy, electron microscopy, UV–vis diffuse reflectance spectroscopy, X-ray photoelectron spectroscopy, etc. Compared with g-C<sub>3</sub>N<sub>4</sub> and commercial P25, the as-prepared photocatalysts exhibit enhanced photocatalytic performance for photoreduction of CO<sub>2</sub> in the presence of water vapor at room temperature. It was found that the mass ratios of urea to Ti(OH)<sub>4</sub> in precursors play a role in formation of the composites, and the high ratios of urea to Ti(OH)<sub>4</sub> result in the composites of g-C<sub>3</sub>N<sub>4</sub> and N-doped TiO<sub>2</sub>, while low ratios only result in N-doped TiO<sub>2</sub>. An interesting selectivity of photocatalytic products displayed that N-doped TiO<sub>2</sub> samples were related to CH<sub>4</sub> and CO generation, while g-C<sub>3</sub>N<sub>4</sub> and N-TiO<sub>2</sub> composites were related to CO generation, and the product selectivity may originate from the formed g-C<sub>3</sub>N<sub>4</sub>. The highest amount of CO (14.73 μmol) was obtained on the optimized photocatalyst under 12 h light irradiation, which is four times of that over commercial P25. Based on these results, a possible mechanism for the enhanced photocatalytic performance was proposed.

© 2014 Elsevier B.V. All rights reserved.

## 1. Introduction

The greenhouse effect as the result of excessive emission of carbon dioxide (CO<sub>2</sub>) into the atmosphere and the energy crisis caused by overexploitation of fossil fuels are recognized to be the two major problems in the foreseeable future [1–3]. Besides the traditional way of emission reduction and energy conservation, the development of renewable energy is also needed. Since the demonstration of photoreduction of CO<sub>2</sub> by Inoue et al. in aqueous suspension to produce hydrocarbon and chemical compounds in 1979 [4], great efforts have been made to develop semiconductor photocatalysts [5–11]. Among the various semiconductor photocatalysts, titanium dioxide (TiO<sub>2</sub>) is the most widely used photocatalyst for solar-fuel production, owing to its availability, photostability and nontoxicity [12]. To further enhance the photocatalytic activity, several routes have been proposed [13], in which

crystal anisotropic growth, doping with ions and heterostructuring of semiconductor photocatalysts are three preferred strategies to modify the crystal structure, electronic structure, lifetime of charge carrier and electron-hole recombination probability [14]. For example, by using hydrofluoric acid as a morphology controlling agent, Yang et al. reported well-defined, high-purity and uniform anatase TiO<sub>2</sub> single crystals with the exposure of a large percentage of reactive facets {001}, which showed promising application in photocatalytic reaction [15]. Zuo et al. synthesized highly stable self-doped Ti<sup>3+</sup>-containing TiO<sub>2</sub> photocatalyst through a one-step combustion method and the as-introduced Ti<sup>3+</sup> extends the photoresponse of TiO<sub>2</sub> photocatalyst to visible region, leading to a high photocatalytic activity for hydrogen production [16]. In addition, efficient inter-electron transfer between MoS<sub>2</sub> and CdS heterogeneous junction was also realized for superior hydrogen generation [17].

From another point of view, in addition to the current inorganic semiconductor materials, the organic semiconductor materials are raising increasing interest, owing to the constructed plastic optoelectronic systems and the chemical structure of polymers can be flexibly tuned for specific applications [18]. Very recently, Wang

<sup>\*</sup> Corresponding author. Tel.: +86 1089731586; fax: +86 1069724721.

<sup>\*\*</sup> Corresponding author. Tel: +86 1089739125; fax: +86 1069724721.

E-mail addresses: [jianggy@cup.edu.cn](mailto:jianggy@cup.edu.cn) (G. Jiang), [zhenzhao@cup.edu.cn](mailto:zhenzhao@cup.edu.cn) (Z. Zhao).

et al. first reported that an organic, metal-free polymeric semiconductor, graphitic carbon nitride ( $g\text{-C}_3\text{N}_4$ ) could be an efficient photocatalyst for hydrogen production in water splitting under visible light, which inspires the photocatalytic system designing in the search for energy production [19]. With mesoporous structure constructed in  $g\text{-C}_3\text{N}_4$ , the enhanced efficiency of hydrogen evolution from photochemical reduction of water was demonstrated, due to the facilitated mass transfer process [20]. Through the photocatalytic or photo-electrochemical process, a same conclusion has also been derived in hydrogen production or photocatalytic conversion of  $\text{CO}_2$  with mesoporous  $g\text{-C}_3\text{N}_4$  as photocatalyst, when urea was used for mesoporous  $g\text{-C}_3\text{N}_4$  photocatalyst preparation [21,22]. Therefore, sunlight harvesting, photocatalytic stability and effective charge transfer ability make  $g\text{-C}_3\text{N}_4$  an excellent candidate for photocatalysis.

To further utilize the advantages of  $g\text{-C}_3\text{N}_4$  and the classic  $\text{TiO}_2$ , the composites of  $\text{TiO}_2$  and  $g\text{-C}_3\text{N}_4$  were proposed ( $g\text{-C}_3\text{N}_4\text{-TiO}_2$ ). In this context,  $g\text{-C}_3\text{N}_4$  modified  $\text{TiO}_2$  nanorod arrays were prepared by using a facile chemical vapor deposition process, and excellent visible light photo-electrocatalytic activity for RhB degradation was achieved, with the absorption spectrum expanded [23]. Visible light active  $g\text{-C}_3\text{N}_4\text{-TiO}_2$  synergistic heterojunction was also synthesized by Sridharan et al. through a thermal transformation methodology and improved photocatalytic activity was observed, owing to the fast electron transfer at the interface of the formed heterojunction [24]. Therefore, combining  $\text{TiO}_2$  with  $g\text{-C}_3\text{N}_4$  to form composite photocatalysts seems to be a possible way to construct heterojunction structure, which may enhance the photoactivity, charge transfer ability and enlarge diversity of photocatalyst system. However, for most reported  $g\text{-C}_3\text{N}_4\text{-TiO}_2$  composites, the preparation often involves a heating process to form  $g\text{-C}_3\text{N}_4$  on the basis of  $\text{TiO}_2$ , and the application is mainly focused on the degradation of organic pollutants and other photo-electrochemical field [23,24]. Up to now, there are few reports on simple methods for one-pot fabrication of  $g\text{-C}_3\text{N}_4\text{-TiO}_2$  composite by using corresponding precursors, not mentioning the application in the photoreduction of  $\text{CO}_2$ . In this study, we report for the first time the synthesis of a series of composites of  $g\text{-C}_3\text{N}_4$  and  $\text{TiO}_2$  with in situ doping of nitrogen in  $\text{TiO}_2$  ( $g\text{-C}_3\text{N}_4\text{-N-TiO}_2$ ) by a facile calcination process with available  $\text{Ti}(\text{SO}_4)_2$  and urea as precursors, and the photocatalytic activities of the as-prepared photocatalysts were investigated for photoreduction of  $\text{CO}_2$  under simulated light irradiation. On this basis, efficient photocatalytic conversion of  $\text{CO}_2$  to CO is

demonstrated. Such a simple synthesis method of  $g\text{-C}_3\text{N}_4\text{-N-TiO}_2$  with in situ doping of nitrogen into  $\text{TiO}_2$  will shed new lights on the designing of highly efficient photocatalysts.

## 2. Experimental

### 2.1. Preparation of $g\text{-C}_3\text{N}_4$

All reagents, including  $(\text{NH}_2)_2\text{CO}$  (AR, Sinopharm Chemical Reagent Beijing Co. LTD),  $\text{Ti}(\text{SO}_4)_2$  (AR, Sinopharm Chemical Reagent Beijing Co. LTD) and  $\text{TiO}_2$  (P25, Degussa Co. Ltd., Germany) are analytical grade and used directly without further purification.

Graphitic carbon nitride ( $g\text{-C}_3\text{N}_4$ ) was synthesized by a facile heating method [25]. In detail, urea was placed in a crucible with a cover under ambient pressure in air. After dried in an oven at  $80^\circ\text{C}$  for 12 h, the crucible with urea was put in a Muffle Furnace and heated to  $550^\circ\text{C}$  for 3 h at a heating rate of  $10^\circ\text{C min}^{-1}$  to complete the reaction. The yellow-colored product was washed with nitric acid (0.1 M) and distilled water to remove residual alkaline species (e.g. ammonia) adsorbed on the sample surface, and then dried at  $80^\circ\text{C}$  overnight.

### 2.2. In situ preparation of $g\text{-C}_3\text{N}_4\text{-N-TiO}_2$ composites

The synthesis of titanium precursor was similar to a modified hydrothermal method [26]. Stoichiometric amounts of urea and  $\text{Ti}(\text{SO}_4)_2$  were dissolved in 50 ml distilled water under stirring to form a white precipitate ( $\text{Ti}(\text{OH})_4$ ) as titanium precursor, the precipitate was recovered by centrifuging process.

The composites of graphitic carbon nitride and nitrogen-doped titanium dioxide composites ( $g\text{-C}_3\text{N}_4\text{-N-TiO}_2$ ) were in situ synthesized by thermal treatment of the well mixed urea and  $\text{Ti}(\text{OH})_4$  in an alumina crucible with a cover at different mass ratios. The mixture was heated to  $550^\circ\text{C}$  for 3 h and then  $580^\circ\text{C}$  for 3 h at a heating rate of  $5^\circ\text{C min}^{-1}$  to obtain the product. The product was washed with nitric acid (0.1 M) and distilled water for several times to remove residual alkaline and sulfate species (e.g. ammonia and  $\text{SO}_4^{2-}$ ) adsorbed on the sample, and then dried at  $80^\circ\text{C}$  overnight to get the final product. The precursors comprise of urea and  $\text{Ti}(\text{OH})_4$  with mass ratios of 10:90, 20:80, 30:70, 40:60, 50:50, 60:40, 70:30 and 80:20 were used to synthesize  $g\text{-C}_3\text{N}_4\text{-N-TiO}_2$  composites by the in situ method mentioned above, and the relevant products were denoted as CT-10, CT-20, CT-30, CT-40, CT-50, CT-60, CT-70,

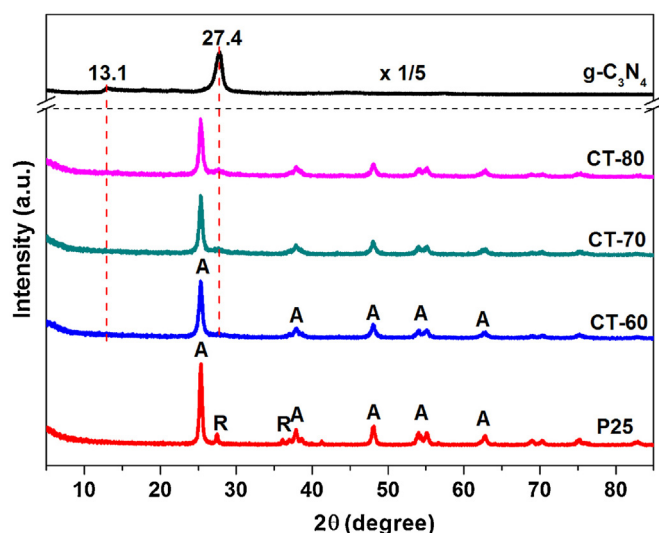


Fig. 1. XRD patterns of  $g\text{-C}_3\text{N}_4$ , CT-60, CT-70, and CT-80 samples. The peaks marked "A" and "R" can be indexed to the anatase and rutile  $\text{TiO}_2$  of P25.

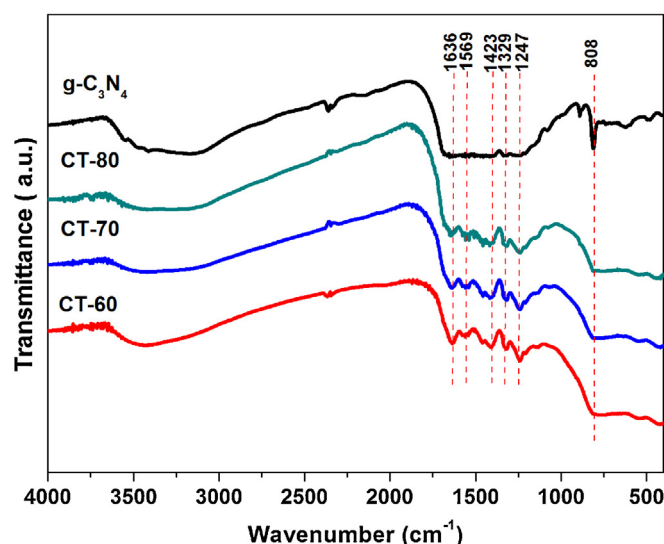


Fig. 2. FT-IR spectra of  $g\text{-C}_3\text{N}_4$ , CT-60, CT-70 and CT-80 samples.

CT-80, correspondingly. P25 and g-C<sub>3</sub>N<sub>4</sub> were chosen as the reference catalysts and their photocatalytic activity were compared with those prepared by the in situ technique.

### 2.3. Characterization

The crystallographic phase of the prepared products were determined by powder X-ray diffraction (Shimadzu XRD 6000) using Cu K $\alpha$  ( $\lambda=0.15406$  nm) radiation with a Nickel filter operating at 40 kV and 10 mA in the  $2\theta$  range of 5–85°. Fourier transform infrared (FT-IR) spectra were obtained by a FTS-3000 spectrophotometer (American Digilab Company). The specific surface areas of the samples were measured by nitrogen sorption at 77 K on Quantachrome Autosorb (IQ) analyzer and calculated by the Brunauer Emmett Teller (BET) method. The morphologies of the samples were observed by a scanning electron microscope (FEI Quanta 2100F) with EDX analysis attachment. Visible Raman spectra were recorded at room temperature on a Renishaw inVia scanning double monochromator with the spectral resolution of 4 cm<sup>-1</sup>. The 532 nm single-frequency laser was used as the excitation source. Transmission electron microscopy (TEM) and high-resolution transmission electron microscopy (HRTEM) images were recorded with a field emission transmission electron microscope (2100, JEOL Co., Japan) operated at an accelerating voltage of 200 kV. X-ray photoelectron spectroscopy (XPS) measurements were carried out with a Perkin-Elmer PHI-1600 ESCA spectrometer using Mg K $\alpha$  ( $h\nu=1253.6$  eV,  $1\text{ eV}=1.603\times10^{-19}$  J) X-ray source. The XPS spectra were calibrated with respect to the binding energy of the C 1s peak at 284.6 eV and deconvoluted using related software. The UV-Vis absorbance and diffuse-reflectance

spectra were performed at room temperature between 200 and 800 nm on a UV-vis spectrophotometer (Hitachi U-4100) with an integrating sphere diffuse reflectance attachment using BaSO<sub>4</sub> as reference. The photoluminescence (PL) spectra of the as-prepared samples were measured using a Hitachi F-4600 fluorescence spectrophotometer.

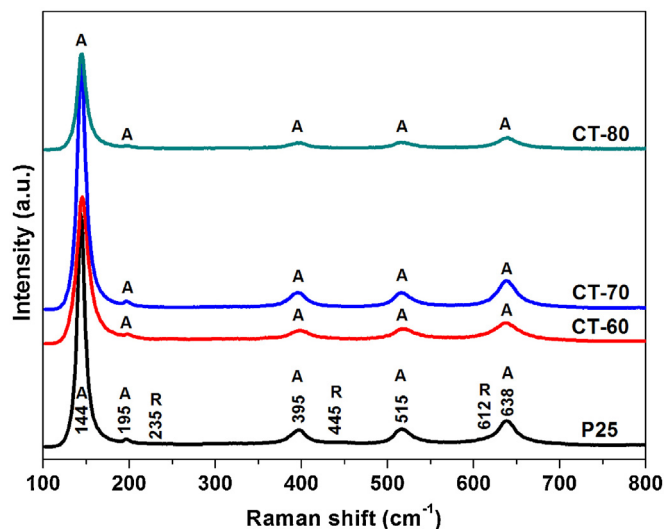


Fig. 3. Raman spectra of the P25, CT-60, CT-70 and CT-80 samples.

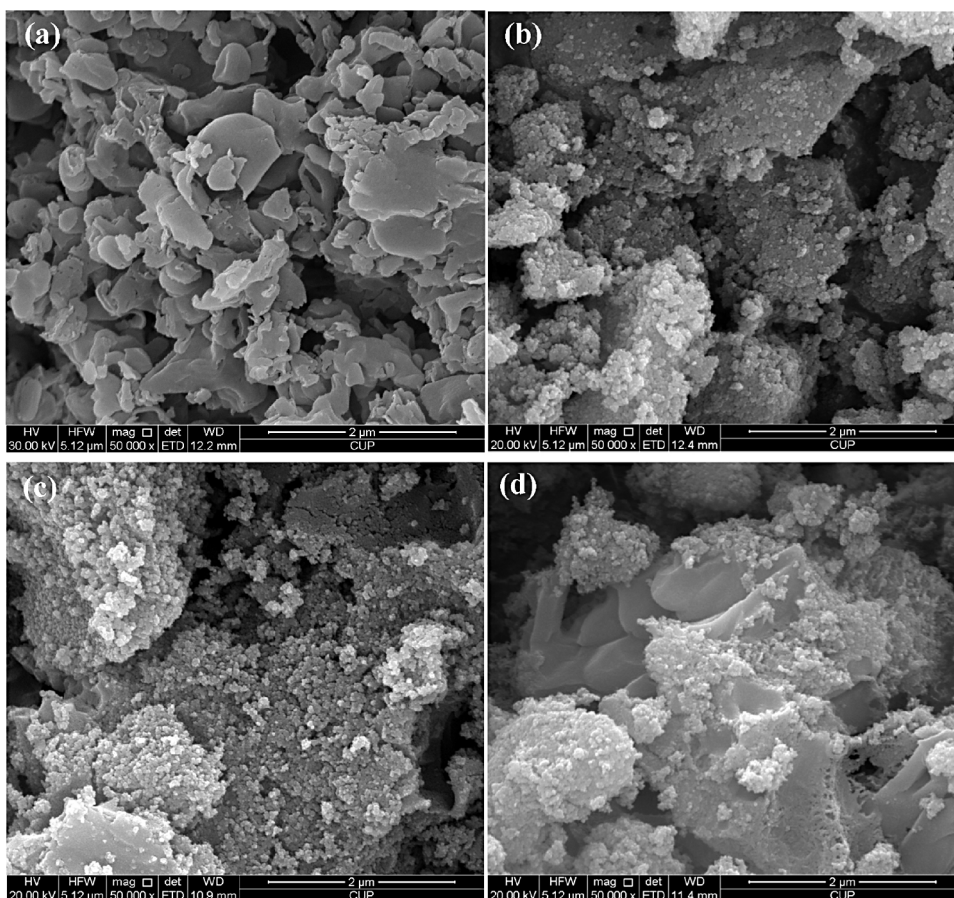


Fig. 4. FE-SEM images of g-C<sub>3</sub>N<sub>4</sub> (a), CT-60 (b), CT-70 (c) and CT-80 (d) samples.

## 2.4. Photocatalytic CO<sub>2</sub> reduction

The photocatalytic reduction of CO<sub>2</sub> experiments were carried out in a gas-closed circulation system, 0.1 g of the tested catalyst was located on a groove of circular Teflon container with an inner basal diameter of 4 cm, which was placed on a porous tray (Figure S1, Supplementary content). A 300 W xenon arc lamp (Perfect Light) was used as the light source of the photocatalytic reaction. Light was passed through a quartz window and the circulated cooling water in quartz window was used to absorb the infrared portion of the Xe lamp to prevent the heating effect of the light source and keep the photoreactor at ambient temperature during the reaction. The intensity of incident light at the location of catalyst was 100 mW/cm<sup>2</sup> measured by a spectroradiometer (FZ-A; Handy, China). The volume of the reaction system was about 780 ml. The reaction setup was vacuum-treated several times, and then the high purity of CO<sub>2</sub> gas was flowed into the reaction setup for reaching ambient pressure. Compressed CO<sub>2</sub> (99.999%, BeiWeng) regulated by a rotor flowmeter (at a flow rate of 15 ml min<sup>-1</sup>) was passed through a deionized water bubbler to introduce CO<sub>2</sub> and water vapor mixture into a photoreactor that

has a quartz window at constant temperature (30 °C). Before irradiation, the as-prepared photocatalysts were kept in the CO<sub>2</sub>–H<sub>2</sub>O atmosphere for 12 h (overnight) to ensure the adsorption equilibrium of gas molecules. During the irradiation, 1 ml of gas was continually taken from the reaction cell at given time intervals (1 h) for subsequent quantitative analysis of product by using an on-line gas chromatograph (GC-9560; HuaAiSePu Corp., China) equipped with two automated gas sampling valves, a thermal conductivity detector (TCD) and two flame ionization detectors (FID). During the photostability measurement, the reaction setup was vacuumed for several times again after the process of 12 h in each run. The quantification of the products was based on the external standard with the use of a calibration curve.

## 3. Results and discussion

### 3.1. Characterization of the as-prepared samples

The samples were characterized by XRD to reveal their phase composition. Fig. 1 shows XRD patterns of the P25, g-C<sub>3</sub>N<sub>4</sub>, CT-60, CT-70, CT-80 composites. Two peaks were found in g-C<sub>3</sub>N<sub>4</sub> at

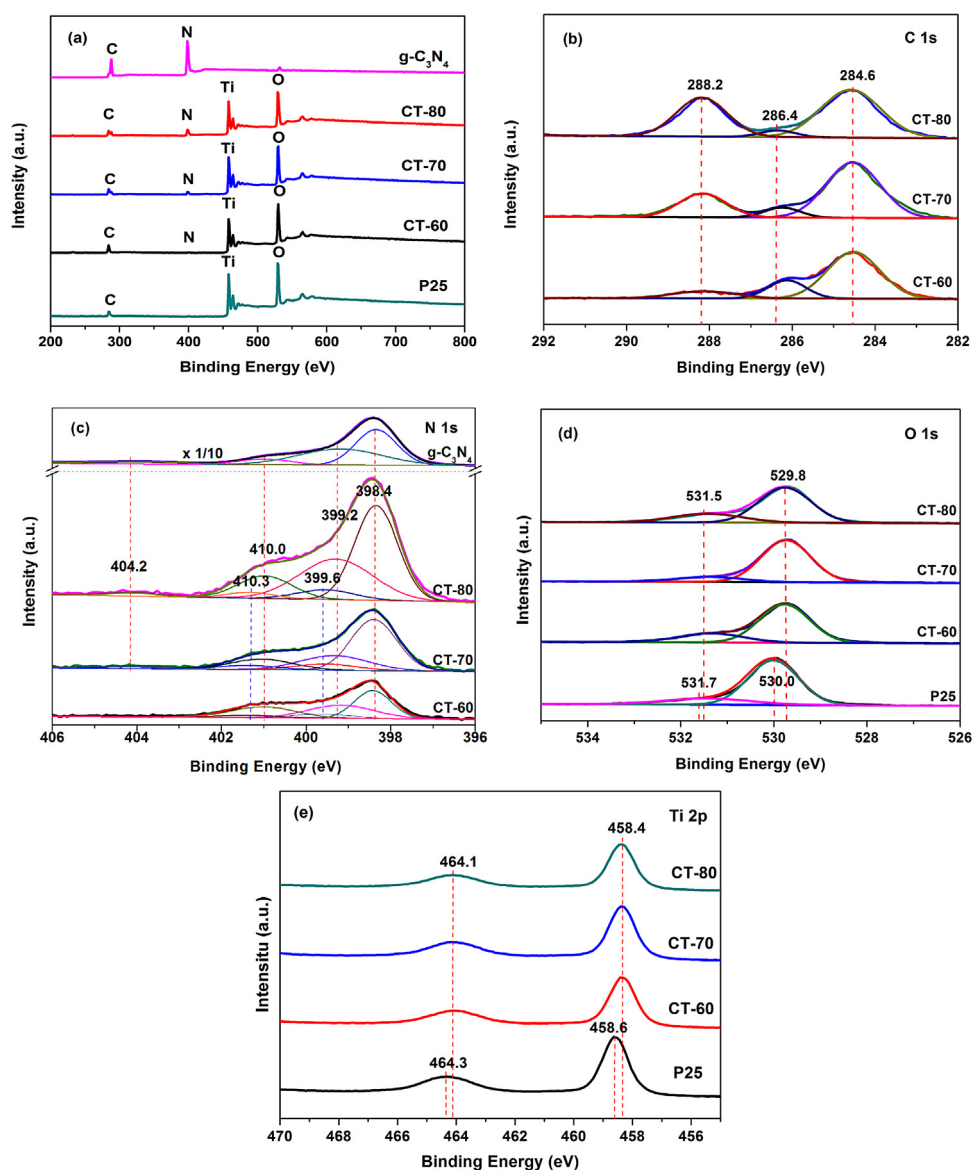


Fig. 5. XPS spectra of P25, g-C<sub>3</sub>N<sub>4</sub>, CT-60, CT-70, CT-80 samples.

around  $13.1^\circ$  (100) and  $27.4^\circ$  (002), which can be indexed to the characteristic in-planar structural packing and inter-planar stacking peaks of the aromatic systems in graphite-like carbon nitride [25,27–29]. The XRD patterns of CT-60, CT-70 and CT-80 samples show some strong peaks attributed to the anatase phase of  $\text{TiO}_2$  and weaker peak (002) attributed to  $\text{g-C}_3\text{N}_4$ , which may be due to its lower content and high dispersity. The peaks marked 'A' and 'R' for P25 can be indexed to the anatase and rutile phase of  $\text{TiO}_2$ , respectively. The (002) peak of CT-80 sample is more distinct than other samples, which may indicate the increased carbon nitride content in this sample. Based on these results, it can be concluded that the CT-60, CT-70, CT-80 composite have a two phase composition of  $\text{g-C}_3\text{N}_4$  and  $\text{TiO}_2$ . In contrast, the CT-10, CT-20, CT-30, CT-40, CT-50 samples show some strong peaks attributed to the anatase phase of  $\text{TiO}_2$  (Fig. S2, Supplementary content), while no distinguishable peaks of  $\text{g-C}_3\text{N}_4$  can be observed, indicating that no  $\text{g-C}_3\text{N}_4$  was formed or no detectable  $\text{g-C}_3\text{N}_4$  existed in these samples.

The formation of  $\text{g-C}_3\text{N}_4$  can be proved by Fourier transform infrared (FT-IR) spectroscopy. Fig. 2 illustrates the FT-IR spectra of  $\text{g-C}_3\text{N}_4$ , CT-60, CT-70 and CT-80 composite. All the samples show the similar characteristic features to the previous results [25,27]. The absorption band centered at  $1636\text{ cm}^{-1}$  can be ascribed to the C–N stretching vibration modes, while the four strong absorption bands centered at 1247, 1329, 1423 and  $1569\text{ cm}^{-1}$  correspond to the typical stretching mode of CN heterocycle [28], the absorption band at  $808\text{ cm}^{-1}$  can be attributed to the out-of-plane ring bending modes of C–N heterocycles [27,28,30–32]. Besides, the broad band at  $500\text{--}750\text{ cm}^{-1}$  of CT-60, CT-70 and CT-80 composite can be attributed to the characteristic peak of  $\text{TiO}_2$  [26], while the broad bands from  $3000\text{ to }3600\text{ cm}^{-1}$  in CT-60, CT-70, CT-80 can be ascribed to the stretching vibrations of –OH group in  $\text{TiO}_2$  and terminal N–H or  $\text{NH}_2$  group stretching vibrations of  $\text{g-C}_3\text{N}_4$  [23], indicating the existence of  $\text{g-C}_3\text{N}_4$  and  $\text{TiO}_2$  in composites. In our experiment, it was also found that no  $\text{g-C}_3\text{N}_4$  was formed when the mass ratio of urea to  $\text{Ti}(\text{OH})_4$  less than 60:40 (Fig. S3, Supplementary content). So the formation of  $\text{g-C}_3\text{N}_4$  strongly depends on the mass ratios of urea to  $\text{Ti}(\text{OH})_4$  during the catalyst preparation.

The crystalline phase of  $\text{TiO}_2$  can also be identified by Raman spectra. Fig. 3 displays the Raman spectra of P25, CT-60, CT-70, CT-80 samples. It can be seen from the Fig. 3 that the anatase phase of P25 shows typical Raman bands at 144, 195, 395, 515 and  $638\text{ cm}^{-1}$ , and rutile phase of P25 shows Raman bands at 143 (Raman band appear at  $143\text{ cm}^{-1}$  superimposed with  $144\text{ cm}^{-1}$  due to the anatase phase), 235, 445,  $612\text{ cm}^{-1}$ , which is in agreement with the literature [33], while the Raman bands in CT-60, CT-70, CT-80 are similar to that of anatase phase in P25, which means the anatase  $\text{TiO}_2$  is formed in CT-60, CT-70 and CT-80. Similar Raman spectra can also be observed in CT-10, CT-20, CT-30, CT-40, CT-50 samples, indicating the formation of anatase phase of  $\text{TiO}_2$  (Fig. S4, Supplementary content).

Fig. 4 shows the FE-SEM images of  $\text{g-C}_3\text{N}_4$  and  $\text{g-C}_3\text{N}_4\text{-N-TiO}_2$  composites. From Fig. 4a, it can be seen that the  $\text{g-C}_3\text{N}_4$  sample shows obvious two dimensional lamellar structures with wrinkles and irregular folding structures, and other samples in Fig. 4b–d shows obvious agglomeration of nanoparticles and tissue-like texture of  $\text{g-C}_3\text{N}_4$  with a quite distinct morphology from that of  $\text{TiO}_2$ . From Fig. 4b–d, it can be also found that the diameter of particles covered on the  $\text{g-C}_3\text{N}_4$  were slowly decreased with the increase of the urea content in precursors, which indicates that the formation of  $\text{g-C}_3\text{N}_4$  could inhibit the growth of nanoparticles. Such a dispersiveness and regulation of  $\text{TiO}_2$  nanoparticles on the surface of  $\text{g-C}_3\text{N}_4$  may provide a good basis for efficient photocatalysis. Further EDX measurements were also performed to get the quantitative analysis results about the as-prepared samples (Fig. S5,

Supplementary content), and the existence of N species were confirmed in all as-prepared samples.

In order to examine the chemical states of elements involved in the as-prepared samples, XPS measurements were performed. Fig. 5a illustrates XPS survey spectra of P25,  $\text{g-C}_3\text{N}_4$ , CT-60, CT-70 and CT-80 samples and elements of C, N, O, Ti were detected. From the XPS spectra of C 1s in Fig. 5b, three peaks centered at 284.6, 286.4 and 288.2 eV can be observed in all three samples. The peak located at 284.6 eV can be assigned to the C–C or adventitious carbon, the peak at 288.2 eV can be ascribed to the N–C=N group of  $\text{g-C}_3\text{N}_4$  [25,34–36], and the peak at 286.4 eV can be attributed to C–O species from the adsorbed  $\text{CO}_2$  and isocyanic acid ( $\text{HN}=\text{C}=\text{O}$ ), or incompletely reacted oxygen-containing intermediates formed during the heating process [25]. Fig. 5c presents the N 1s spectra of CT-60, CT-70 and CT-80 samples. A broad peak extending from 397 to 403 eV is observed for all the samples, which can be fitted into three strong peaks with binding energy at 398.4, 399.2, 401.0 eV and two weak peaks at 401.3, 399.6 eV. The N1s binding energy of 398.4 eV can be ascribed to N–C=N group of  $\text{g-C}_3\text{N}_4$ , two peaks at 399.2 and 401.0 eV can be attributed to N–(C)<sub>3</sub> and C–N–H groups of  $\text{g-C}_3\text{N}_4$  [25,34,37]. The other two peaks at 399.6 and 401.3 eV are attributed to the N atoms located at the interstitial sites of  $\text{TiO}_2$  lattice and the O–Ti–N sites incorporated into

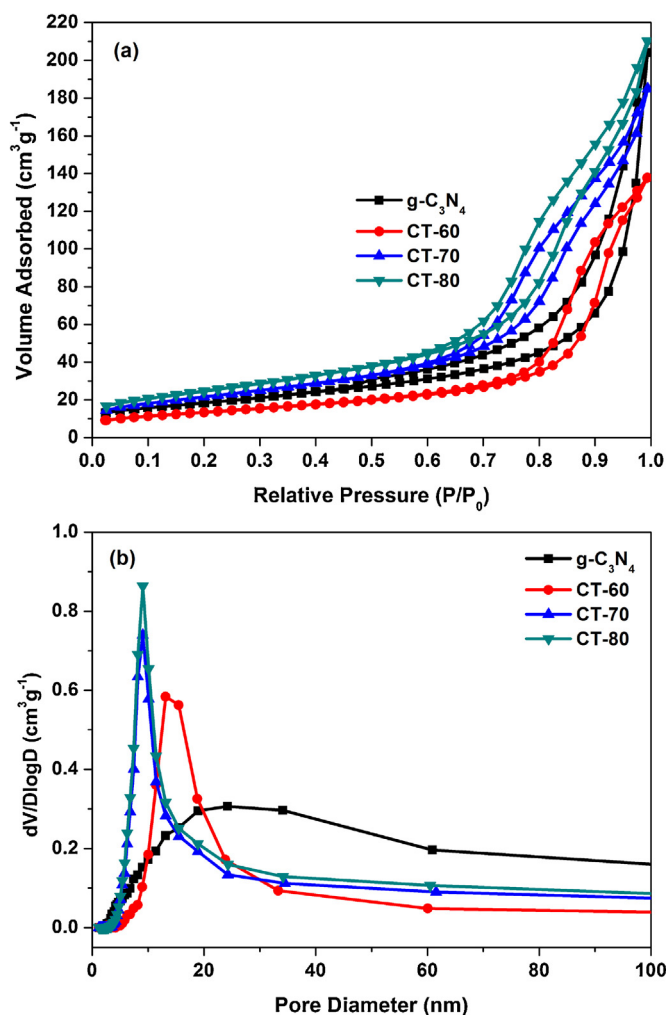


Fig. 6.  $\text{N}_2$  adsorption-desorption isotherm (a) and corresponding Barrett-Joyner-Halenda (BJH) pore-size distribution plots (b) of  $\text{g-C}_3\text{N}_4$ , and CT-60, CT-70, CT-80 samples.

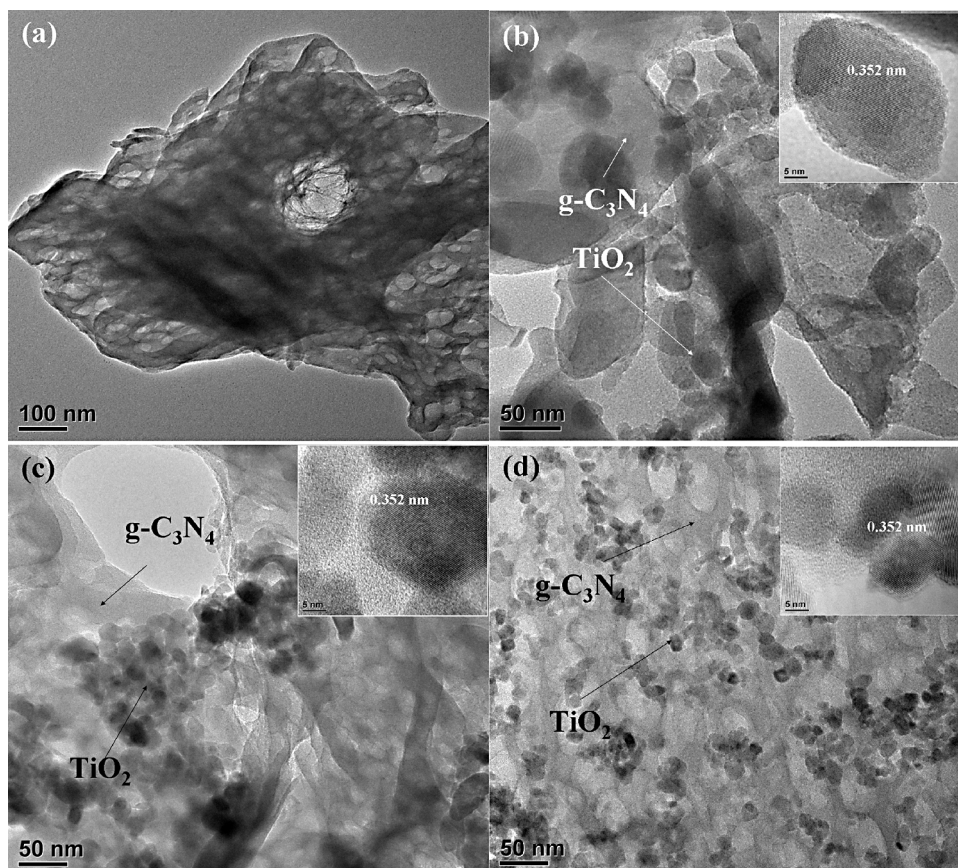
the  $\text{TiO}_2$  lattice, respectively. In combination with the results of XRD, FT-IR, Raman and EDX mentioned above, it could confirm the incorporation of nitrogen species into  $\text{TiO}_2$  and the formation of N-doped  $\text{TiO}_2$  during the heating process [38,39]. For  $\text{g-C}_3\text{N}_4$ , CT-70 and CT-80 samples, another weak peak located at 404.2 eV in Fig. 5c is attributed to the charging effects or positive charge localization in the heterocycles [40]. The O 1s spectra (Fig. 5d) show two peaks of the binding energy at 529.8 and 531.5 eV, which is associated with the  $\text{O}^{2-}$  in  $\text{TiO}_2$  and the  $-\text{OH}$  group on the surface of samples [41,42]. From Fig. 5e, Ti 2p peaks can be observed at binding energy of 464.1 ( $\text{Ti } 2p_{1/2}$ ) and 458.4 eV ( $\text{Ti } 2p_{3/2}$ ) [41–44]. Compared with Ti  $2p_{3/2}$  peak at 458.6 eV in P25, a little shift of 0.2 eV in CT-60, CT-70, CT-80 can be observed in Fig. 5e, which is because the electronic structure of Ti species in the composites may be changed by doping of heteroatom and the formation of  $\text{g-C}_3\text{N}_4$ . Based on above analysis, it comes to the conclusion that the  $\text{g-C}_3\text{N}_4$ - $\text{TiO}_2$  composites were successfully synthesized with in situ doping of nitrogen into  $\text{TiO}_2$  during the heating process. The XPS spectra of CT-10, CT-20, CT-30, CT-40, CT-50 were also performed to further investigate the chemical stated of N 1s, O 1s and Ti 2p in these samples and corresponding results were obtained (Fig. S6, Supplementary content), and the N doping was determined.

To analyze the textural properties of the as-prepared samples, the  $\text{N}_2$  adsorption–desorption isotherms at 77 K were measured. The calculated BET specific surface area of  $\text{g-C}_3\text{N}_4$  is  $65.2 \text{ m}^2 \text{ g}^{-1}$ , and the specific surface areas of CT-60, CT-70, CT-80 samples are 47.9, 78.2,  $89.3 \text{ m}^2 \text{ g}^{-1}$ , respectively. From Fig. 6a, H4 type hysteresis loops can be observed in the  $\text{N}_2$  adsorption–desorption isotherms obtained from the samples, indicating the formation of mesopores embedded in the matrix. Fig. 6b presents the distribution of pore diameter of  $\text{g-C}_3\text{N}_4$ , CT-60, CT-70 and CT-80 samples.

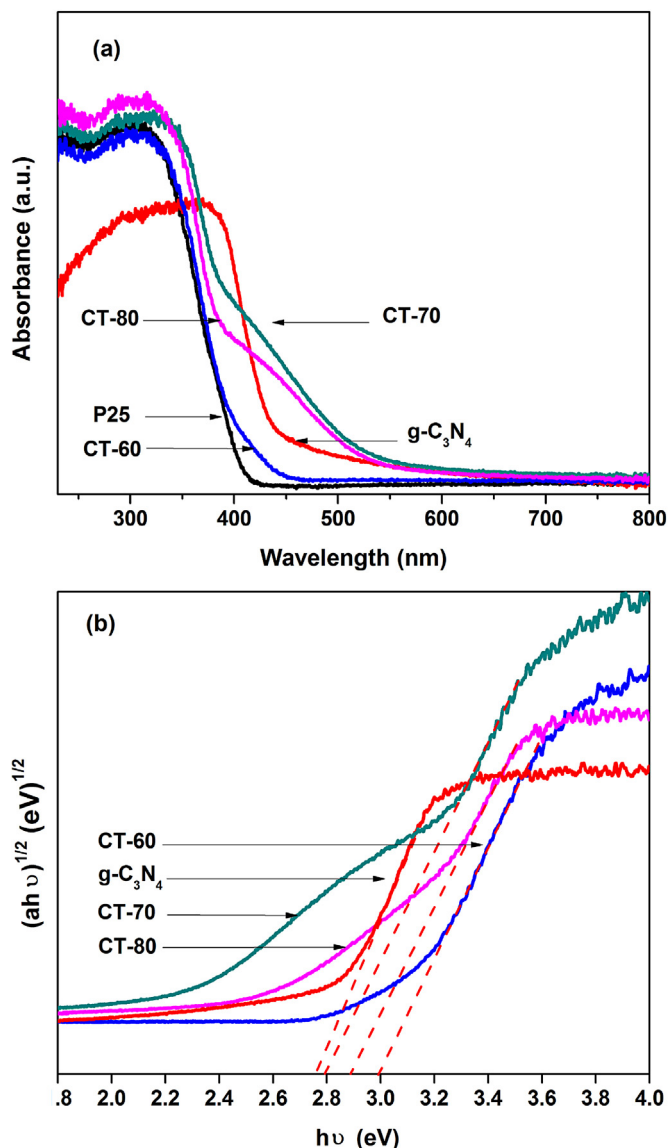
From Fig. 6b, it can be observed that the average pore diameter of  $\text{g-C}_3\text{N}_4$  is about 20–40 nm, while the average pore diameters of CT-60, CT-70 and CT-80 are centered at 15, 10, 10 nm, respectively, indicating that the urea employed in precursors can create mesopore during the heating process. The broad pore size distribution derived from the carbonization of urea and corresponding intermediate polymerization process, while the narrow peak may be caused by the aggregation of  $\text{TiO}_2$  nanoparticles in the mesopore of  $\text{g-C}_3\text{N}_4$ .

Fig. 7 shows the TEM images of  $\text{g-C}_3\text{N}_4$ , CT-60, CT-70, CT-80 samples after ultrasonic treatment of 4 h. From Fig. 7a, it can be clearly seen that the  $\text{g-C}_3\text{N}_4$  presents obvious mesoporous sheet structure. The TEM images of  $\text{g-C}_3\text{N}_4$  and N- $\text{TiO}_2$  composites (CT-60, CT-70, CT-80) are shown in Fig. 7b–d, respectively, which displayed the sheet structure with the agglomeration of nanoparticles on the surface of  $\text{g-C}_3\text{N}_4$ . The HRTEM images of CT-60, CT-70 and CT-80 samples (insets) clearly show an interplanar spacing of 0.352 nm, which confirmed the formation of  $\text{TiO}_2$  nanoparticles (1 0 1). From Fig. 7b–d, it can also be estimated that the particle size of  $\text{TiO}_2$  decreases from CT-60 to CT-80, indicating that the dispersiveness of  $\text{TiO}_2$  nanoparticles on  $\text{g-C}_3\text{N}_4$  can be regulated by changing the urea content during the catalyst preparation. It should be noted that the composite structure of  $\text{g-C}_3\text{N}_4$ - $\text{TiO}_2$  keeps unchanged after the 4 h ultrasonic treatment, indicating a firm connection exists between  $\text{TiO}_2$  nanoparticles and  $\text{g-C}_3\text{N}_4$ , which may be favorable for the photo-induced charge transfer and thus provide a good basis for the after-mentioned photocatalysis.

Fig. 8 depicts the absorbance spectra of P25,  $\text{g-C}_3\text{N}_4$ , CT-60, CT-70, CT-80 and Kubelka–Munk transformed reflectance spectra of  $\text{g-C}_3\text{N}_4$ , CT-60, CT-70, CT-80. It can be seen from Fig. 8a that there is a clear red shift of the absorption in CT-60, CT-70, CT-80 samples,



**Fig. 7.** TEM images of  $\text{g-C}_3\text{N}_4$  (a), CT-60 (b), CT-70 (c), CT-80 (d) samples. Insets show the HRTEM images of  $\text{TiO}_2$  nanoparticles with interplanar spacing of 0.352 nm.



**Fig. 8.** UV-vis absorbance spectra of P25, g-C<sub>3</sub>N<sub>4</sub>, and CT-60, CT-70, CT-80 composites (a), Kubelka–Munk transformed reflectance spectra and estimated optical absorption bandgap of g-C<sub>3</sub>N<sub>4</sub>, and CT-60, CT-70, CT-80 samples (b). The band gap energy of as-prepared samples can be calculated from UV-vis diffuse reflectance spectra, according to the equation:  $(\alpha h\nu)^n = A(h\nu - E_g)$ , in which  $\alpha$ ,  $\nu$ ,  $A$ , and  $E_g$  are the absorption coefficient, light frequency, proportionality constant and bandgap, respectively [23]. The value of  $n$  depends on the property of materials. For g-C<sub>3</sub>N<sub>4</sub>, the  $n$  is 1/2 for the indirect band gap semiconductor.

in comparison with that of commercial P25, and the as-prepared samples show obvious light absorption in visible light region, with the absorption edge of CT-60, CT-70, CT-80 up to 435, 520, 500 nm, which may due to the existence of g-C<sub>3</sub>N<sub>4</sub> and nitrogen species. With increasing amount of urea in precursors during the heating process, the absorption edge of the CT-70, CT-80 shift remarkably to long wavelength and the existence of g-C<sub>3</sub>N<sub>4</sub> may contribute to this result. Fig. 8b depicts the Kubelka–Munk transformed reflectance spectra and estimated optical absorption bandgaps of g-C<sub>3</sub>N<sub>4</sub>, CT-60, CT-70, CT-80. The band gap of g-C<sub>3</sub>N<sub>4</sub> is evaluated to be 2.74 eV, and the band gaps for CT-60, CT-70 and CT-80 composites are estimated to be 2.98, 2.79 and 2.89 eV, respectively, which are smaller than that of P25. Therefore, the formation of g-C<sub>3</sub>N<sub>4</sub>, N doping and the interaction between g-C<sub>3</sub>N<sub>4</sub> and N-TiO<sub>2</sub> in heterojunction may contribute to the narrowing of the bandgap, due to the modified electronic structures of the photocatalyst matrix, which is in

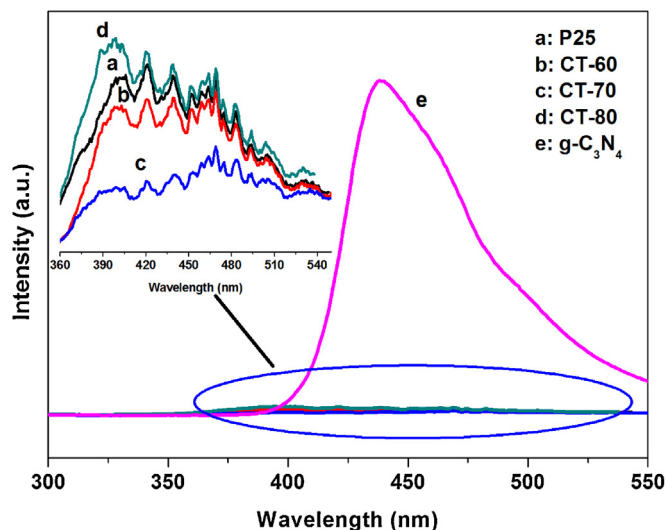


**Fig. 9.** Photoluminescence spectra of P25, g-C<sub>3</sub>N<sub>4</sub>, CT-60, CT-70 and CT-80 samples. Inset shows the detailed emission peaks of P25, CT-60, CT-70 and CT-80 samples.

good agreement with the XPS spectra. Interestingly, the bandgap of CT-70 is 0.1 eV lower than that of CT-80, and the suitable N and g-C<sub>3</sub>N<sub>4</sub> content in composites and the interaction between them could contribute to the best photoresponsive ability and the narrowest bandgap among the as-prepared photocatalysts, although the content of g-C<sub>3</sub>N<sub>4</sub> in CT-80 is increased. In contrast, unlike the samples prepared with the mass ratios of urea to Ti(OH)<sub>4</sub> higher than 50:50 during catalyst preparation, the samples prepared at lower ratios mainly absorb the light in ultraviolet region, with part of the absorption edge extended to visible light, to some extent (Fig. S7, Supplementary content).

To understand the trapping, immigration and transfer property of electron–hole pairs, photoluminescence (PL) emission measurements were applied and PL spectra were recorded. It is known that the intensity of the PL emission spectra depend on the recombination of excited electrons and holes, the lower the PL emission intensity, the lower the recombination property of the samples [23]. Fig. 9 shows the PL spectra of P25, g-C<sub>3</sub>N<sub>4</sub>, CT-60, CT-70 and CT-80 samples. It can be observed that the g-C<sub>3</sub>N<sub>4</sub> shows the strongest emission peak at about 440 nm at ambient temperature, which is equivalent to the bandgap energy of 2.74 eV. In comparison with that of g-C<sub>3</sub>N<sub>4</sub>, the emission intensities of CT-60, CT-70, CT-80 are much lower, indicating that good separation of electrons and holes is achieved by introducing nitrogen-doped TiO<sub>2</sub> in g-C<sub>3</sub>N<sub>4</sub>. From the inset in Fig. 9, it can be seen that with increased ratios of urea to Ti(OH)<sub>4</sub> during the catalyst preparation, the emission intensity in CT-60 and CT-70 samples decreases. Among the as-prepared composites, CT-70 demonstrates the lowest emission intensity, i.e., the lowest recombination efficiency. With further increasing the content of urea in precursors, the emission intensity increases, which indicates that the good separation ability of electrons and holes depends on a suitable content of g-C<sub>3</sub>N<sub>4</sub> and the formation of heterojunction structure in composites, while excessive g-C<sub>3</sub>N<sub>4</sub> in composite may form recombination center.

### 3.2. Evaluation of photocatalytic activity

The photocatalytic reduction was carried out in a gas-closed circulation system operated under simulated light irradiation with photocatalyst, CO<sub>2</sub>, water vapor sealed in the system. Samples were continually taken from the reaction cell at given intervals (1 h) for subsequent quantitative analysis that based on the external

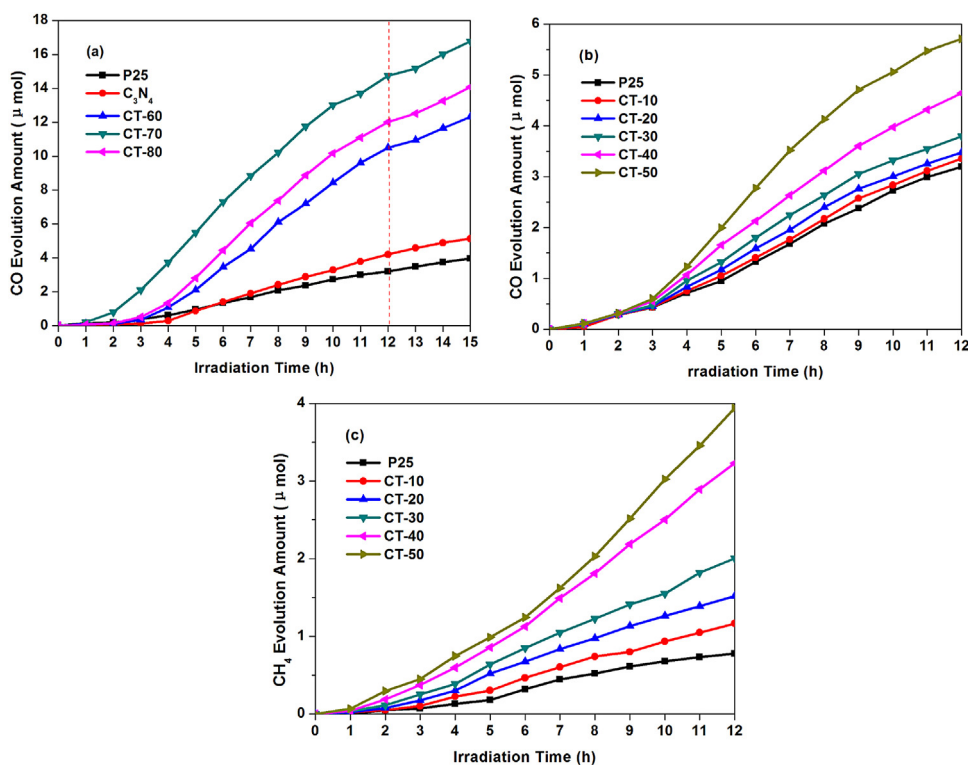


**Fig. 10.** CO generation over P25, g-C<sub>3</sub>N<sub>4</sub>, and CT-60, CT-70, CT-80 samples as a function of UV–vis light irradiation time (a), CO generation over P25, CT-10, CT-20, CT-30, CT-40, CT-50 samples as a function of UV–vis light irradiation time (b) and CH<sub>4</sub> generation over P25, CT-10, CT-20, CT-30, CT-40, CT-50 samples as a function of UV–vis light irradiation time (c).

standard method and calibration curve. Commercial P25 was selected as the reference catalyst in photoreduction of CO<sub>2</sub>.

During the evaluation test, an interesting phenomenon was observed. The products of photoreduction of CO<sub>2</sub> in the presence of water vapor highly depend on the as-prepared photocatalysts. For g-C<sub>3</sub>N<sub>4</sub> and CT-60, CT-70, CT-80 samples, the product is only CO, while for P25, CT-10, CT-20, CT-30, CT-40 and CT-50 samples, the main products are CO and CH<sub>4</sub>. Fig. 10a shows the photocatalytic activity of P25, g-C<sub>3</sub>N<sub>4</sub> and CT-60, CT-70, CT-80 samples in photoreduction of CO<sub>2</sub> process with CO as reduced product. It can be seen from Fig. 10a that the evolved CO amount over the commercial P25 is 3.19 μmol after 12 h light irradiation, while CO amount over g-C<sub>3</sub>N<sub>4</sub> is determined to be 4.20 μmol under 12 h light irradiation. Compared with P25 and g-C<sub>3</sub>N<sub>4</sub> samples, CO amounts over CT-60, CT-70, CT-80 samples are markedly increased. It is reported that CO could be produced on g-C<sub>3</sub>N<sub>4</sub> during photocatalytic reaction under light irradiation in the presence of water vapor [45], and the formation of g-C<sub>3</sub>N<sub>4</sub> in CT-60, CT-70, CT-80 may play a role in enhancing CO evolution. Meantime, the heterojunction between g-C<sub>3</sub>N<sub>4</sub> and nitrogen-doped TiO<sub>2</sub> promotes the separation of light-induced electrons and holes. Consequently, the as-prepared composites demonstrate enhanced catalytic performance. Among the as-prepared samples, CT-70 presents the highest CO evolution amount (14.73 μmol) during light irradiation, which is in line with previous results that CT-70 has the best visible light absorption and lowest recombination efficiency of electrons and holes. It can also be observed that the CO amounts over CT-60, CT-70 and CT-80 samples are enhanced with a prolonged irradiation time, and a slight decrease in the production rate occurs upon prolonged irradiation time, indicating that some intermediates may be aggregated and covered on the active site of photocatalysts [41,44].

Fig. 10b and c shows the amounts of CO and CH<sub>4</sub> achieved on P25, CT-10, CT-20, CT-30, CT-40, CT-50, respectively. During the 12 h

light irradiation, it can be seen that the amounts of CO on the CT-10, CT-20, CT-30, CT-40, CT-50 were 3.35, 3.47, 3.79, 4.64, 5.71 μmol, and the amount of CH<sub>4</sub> of 1.17, 1.52, 2.00, 3.23, 3.94 μmol were obtained simultaneously. Based on these results, it can be found that the product selectivity depends on the content of g-C<sub>3</sub>N<sub>4</sub> in composites, that is, when the mass ratios of urea to Ti(OH)<sub>4</sub> are higher than 50:50, corresponding to g-C<sub>3</sub>N<sub>4</sub> and N-TiO<sub>2</sub> composites, only CO is generated as the reduced product, while CO and CH<sub>4</sub> can be obtained on N-TiO<sub>2</sub> samples with preparation ratios of urea to Ti(OH)<sub>4</sub> lower than 60:40. So the photocatalytic activity and product selectivity can be facily regulated by changing the

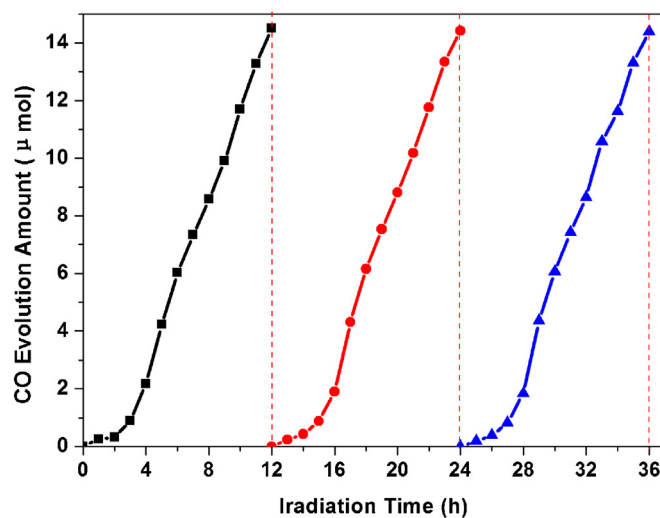


**Fig. 11.** Stability study of photocatalytic CO evolution over the CT-70 sample. Condition: 0.1 g catalyst, constant pressure, ambient temperature, 300 W Xe-lamp for the UV–vis light irradiation.

ratios of urea to  $\text{Ti}(\text{OH})_4$  during catalyst preparation. Besides, all the prepared samples showed better photocatalytic activity than P25, which may come to a conclusion that the present in situ synthetic method was an efficient way to produce photocatalysts with better photocatalytic activity, when  $\text{g-C}_3\text{N}_4$  was selected as photosensitizer.

During the evaluation of photocatalysts, controlled experiments were performed, and the results showed that no appreciable amount of reduced products can be detected in the absence of photocatalysts or light irradiation, illustrating that the present reaction is a photocatalytic process. Additionally, neither CO or  $\text{CH}_4$ , nor other carbon compounds can be detected by introducing Ar instead of  $\text{CO}_2$  through bubbling into photocatalytic system or direct introducing  $\text{CO}_2$  into the reaction setup in the absence of  $\text{H}_2\text{O}$  under light irradiation, indicating that CO and  $\text{CH}_4$  were originated from  $\text{CO}_2$  in the presence of  $\text{H}_2\text{O}$  under light irradiation.

To investigate the photostability of as-prepared samples, CT-70 sample was selected to carry out consecutive photocatalytic reactions. Fig. 11 shows the photostability of the CT-70 during consecutive runs of 36 h light irradiation with fresh  $\text{CO}_2$  and  $\text{H}_2\text{O}$  periodically replaced in each run. As depicted in Fig. 11, no deactivation was observed for the CT-70 photocatalyst along with the extending reaction time, indicating the good photostability of CT-70 sample.

### 3.3. Possible photocatalytic mechanism

As described above, compared with the  $\text{g-C}_3\text{N}_4$  and commercial P25, the enhancement of photocatalytic activity of CT-60, CT-70 and CT-80 samples were mainly due to the band regulation, light sensitization, and high efficiency of charge separation induced by the formed heterojunction between  $\text{g-C}_3\text{N}_4$  and  $\text{N-TiO}_2$  during the in situ synthesis process. And the matched CB potentials, the doped energy level formed in  $\text{N-TiO}_2$  also contribute to the enhanced performance of the composites. Fig. 12a describes the possible reaction mechanism for the formation of CO over composite photocatalysts under light irradiation. It is known that the photocatalytic selectivity generally depends on the structure properties of the photocatalysts and the reaction conditions [41,46]. During the photoreduction process, eight electrons are required in the formation of each  $\text{CH}_4$  molecule [8,9], while only two electrons are needed for each CO molecule evolution [45,46]. Therefore, the photoreduction of  $\text{CO}_2$  to CO may be a dynamic favored process in the present system. Under simulated light irradiation, electrons and holes are generated and transferred between the interface of  $\text{g-C}_3\text{N}_4$  and  $\text{N-TiO}_2$ . The holes formed in  $\text{g-C}_3\text{N}_4$  and transferred from the VB of  $\text{TiO}_2$  may oxidize  $\text{H}_2\text{O}$  molecules absorbed on the surface of  $\text{g-C}_3\text{N}_4$  to generate  $\text{O}_2$  and protons. The photogenerated electrons in  $\text{N-TiO}_2$  and the electrons transferred from  $\text{g-C}_3\text{N}_4$  could reduce  $\text{CO}_2$  molecules to C1 intermediates. The absence of  $\text{CH}_4$  on samples of CT-60, CT-70 and CT-80 suggests that the protons may fail to capture the photogenerated electrons, but fall into the formed electron-rich aromatic heterocycles of  $\text{g-C}_3\text{N}_4$  in photocatalytic reaction, where the protons could be stabilized by the conjugated aromatic system and thus they are hard to participate in the evolution process of  $\text{CH}_4$ . And the electrons in the CB of  $\text{g-C}_3\text{N}_4$  can transfer quickly to the CB of  $\text{N-TiO}_2$  for  $\text{CO}_2$  reduction to CO. Therefore, the formed  $\text{g-C}_3\text{N}_4$ - $\text{N-TiO}_2$  heterojunction can selective photoreduction of  $\text{CO}_2$  to CO in the present system. In contrast, for CT-10 to CT-50 samples, due to the absence of conjugated aromatic system,  $\text{H}^+$  or  $\text{H}^\bullet$  radicals generated in photocatalytic reaction may quickly consumed by  $\text{CO}_2$  in the photocatalytic process and thus  $\text{CH}_4$  and CO were simultaneous detected (Fig. 12b).

To confirm the proposed mechanism, further photocatalytic reactions for  $\text{CO}_2$  reduction were designed. Photocatalytic reduction of  $\text{CO}_2$  in the presence of water vapor was performed on CT-70

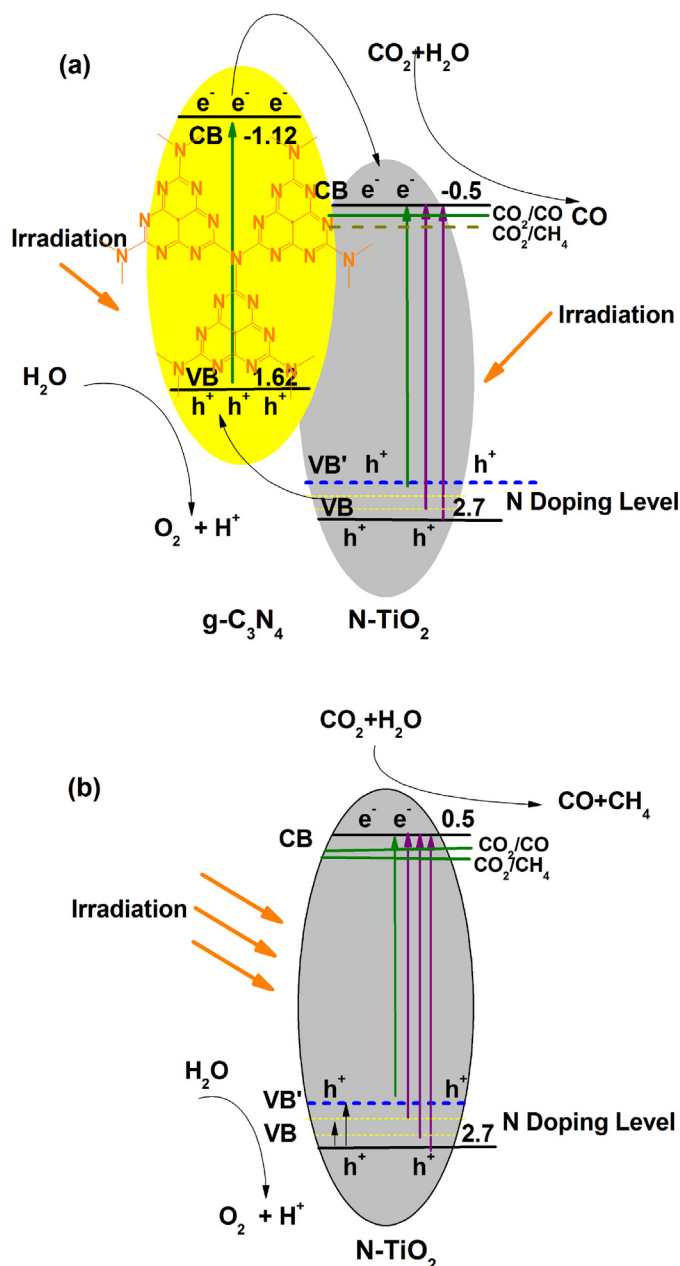


Fig. 12. The proposed mechanism for the photoreduction of  $\text{CO}_2$  over  $\text{g-C}_3\text{N}_4$  and  $\text{N-TiO}_2$  composites (a) and  $\text{N-TiO}_2$  (b).

by injecting  $\text{H}_2$  into present system, and the results were shown in Fig. S8. From Fig. S8, it can be observed that both CO and  $\text{CH}_4$  can be obtained under light irradiation. This result agrees well with our suggested mechanism that  $\text{CH}_4$  can be obtained in a H species-rich system, while only CO can be produced when  $\text{g-C}_3\text{N}_4$  was formed in composites.

## 4. Conclusions

The composites of graphitic- $\text{C}_3\text{N}_4$  and  $\text{N-TiO}_2$  were in situ synthesized by a facile heating method. The formation of  $\text{g-C}_3\text{N}_4$  and doping of nitrogen species into  $\text{TiO}_2$  subcomponent in the composite photocatalysts endow them good visible light sensitization and high efficiency of charge separation during light irradiation. The as-prepared photocatalysts demonstrate good photocatalytic performance and photostability in photoreduction of  $\text{CO}_2$  in the presence of water vapor, and the highest CO evolution amount of

14.73  $\mu\text{mol}$  was achieved on the optimized sample under 12 h light irradiation. The photocatalytic products highly depend on the compositions of the as-prepared catalysts, that is, CO and CH<sub>4</sub> were produced on N-TiO<sub>2</sub> samples, while CO was prone to be formed on g-C<sub>3</sub>N<sub>4</sub> and N-TiO<sub>2</sub> composites. And the specific composition of the as-prepared catalysts could be regulated by varying the mass ratios of urea to Ti(OH)<sub>4</sub> during catalyst preparation, i.e., N-doped TiO<sub>2</sub> was achieved at low ratios, while g-C<sub>3</sub>N<sub>4</sub> and N-TiO<sub>2</sub> composite were produced at high ones. Such a facile regulation of catalyst compositions and the tuning of the photocatalytic selectivity by varying the preparation parameter helps to provide new insights for the design and development of highly efficient photocatalysts in the photoreduction of CO<sub>2</sub> and H<sub>2</sub>O.

## Acknowledgements

This work is financially supported by Prospect Oriented Foundation of China University of Petroleum, Beijing (Grant No. QZDX-2011-02), the National Science Foundation of China (Grant No. U1162117), Beijing Nova Program (Grant No. Z11111005450000), PetroChina Innovation Foundation (2011D-5006-0403).

## Appendix A. Supplementary data

Supplementary data associated with this article can be found, in the online version, at <http://dx.doi.org/10.1016/j.apcatb.2014.03.037>.

## References

- [1] U.A. Joshi, A. Palasyuk, D. Arney, P.A. Maggard, *Journal of Physical Chemistry Letters* 1 (2010) 2719–2726.
- [2] S.C. Roy, O.K. Varghese, M. Paulose, C.A. Grimes, *ACS Nano* 4 (2010) 1259–1278.
- [3] G. Centi, S. Perathoner, *ChemSusChem* 3 (2010) 195–208.
- [4] T. Inoue, A. Fujishima, S. Konishi, K. Honda, *Nature* 277 (1979) 637–638.
- [5] M. Anpo, H. Yamashita, Y. Ichihashi, Y. Fujii, M. Honda, *Journal of Physical Chemistry B* 101 (1997) 2632–2636.
- [6] Y. Shiota, K. Ikeue, M. Ogawa, M. Anpo, *Applied Catalysis A: General* 254 (2003) 251–259.
- [7] Y. Yamada, K. Yano, Q. Xu, S. Fukuzumi, *Journal of Physical Chemistry C* 114 (2010) 16456–16462.
- [8] S.C. Yan, S.X. Ouyang, J. Gao, Z.G. Zou, *Angewandte Chemie International Edition* 49 (2010) 6400–6404.
- [9] Q. Liu, Y. Zhou, J. Kou, X. Chen, Z. Tian, J. Gao, S.C. Yan, Z.G. Zou, *Journal of the American Chemical Society* 132 (2010) 14385–14387.
- [10] P. Li, S.X. Ouyang, G.C. Xi, T. Kako, J.H. Ye, *Journal of Physical Chemistry C* 116 (2012) 7621–7628.
- [11] N. Zhang, S.X. Ouyang, T. Kako, J.H. Ye, *Chemical Communications* 48 (2012) 1269–1271.
- [12] M.R. Hoffmann, S.T. Martin, W.Y. Choi, D.W. Bahnemann, *Chemical Reviews* 95 (1995) 69–96.
- [13] M.D. Hernandez-Alonso, F. Fresno, S. Suarez, J.M. Coronado, *Energy & Environmental Science* 2 (2009) 1231–1257.
- [14] G. Liu, L.Z. Wang, H.G. Yang, H.M. Cheng, G.Q. Lu, *Journal of Materials Chemistry* 20 (2010) 831–843.
- [15] H.G. Yang, C.H. Sun, S.Z. Qiao, J. Zou, G. Liu, *Nature* 453 (2008) 638–641.
- [16] F. Zuo, L. Wang, T. Wu, Z.Y. Zhang, D. Borchardt, P.Y. Feng, *Journal of the American Chemical Society* 132 (2010) 11856–11857.
- [17] X. Zong, H.J. Yan, G.P. Wu, G.J. Ma, F.Y. Wen, L. Wang, C. Li, *Journal of the American Chemical Society* 130 (2008) 7176–7177.
- [18] S.R. Forrest, M.E. Thompson, *Chemical Reviews* 109 (2007) 923–925.
- [19] X.C. Wang, K. Maeda, A. Thomas, K. Takanabe, G. Xin, *Nature Materials* 8 (2009) 76–80.
- [20] X.C. Wang, K. Maeda, X.F. Chen, K. Takanabe, K. Domen, Y.D. Hou, X.Z. Fu, M. Antonietti, *Journal of the American Chemical Society* 131 (2009) 1680–1681.
- [21] Y.W. Zhang, J.H. Liu, G. Wu, W. Chen, *Journal of Materials Chemistry* 4 (2012) 5300–5303.
- [22] J. Mao, T.Y. Peng, Z.H. Zhang, K. Li, L.Q. Ye, L. Zan, *Catalysis Science & Technology* 3 (2013) 1253–1260.
- [23] J. Wang, W.D. Zhang, *Electrochimica Acta* 71 (2012) 10–16.
- [24] K. Sridharan, E.Y. Jang, T.J. Park, *Applied Catalysis B: Environmental* 142–143 (2013) 718–728.
- [25] J.H. Liu, T.K. Zhang, Z.C. Wang, G. Dawson, W. Chen, *Journal of Materials Chemistry* 21 (2011) 14398–14401.
- [26] R.Q. Tan, Y. He, Y.F. Zhu, B.Q. Xu, L.L. Cao, *Journal of Materials Chemistry* 38 (2003) 3973–3978.
- [27] J.X. Sun, Y.P. Yuan, L.G. Qiu, X. Jiang, A.J. Xie, Y.H. Shen, J.F. Zhu, *Dalton Transactions* 41 (2012) 6756–6763.
- [28] S.C. Yan, Z.S. Li, Z.G. Zou, *Langmuir* 25 (2009) 10397–10401.
- [29] A. Thomas, A. Fischer, F. Goettmann, M. Antonietti, J.O. Müller, R. Schlögl, J.M. Carlsson, *Journal of Materials Chemistry* 18 (2008) 4893–4908.
- [30] Y.J. Zhang, A. Thomas, M. Antonietti, X.C. Wang, *Journal of the American Chemical Society* 131 (2009) 50–51.
- [31] Y.J. Wang, R. Shi, J. Lin, Y.F. Zhu, *Energy & Environmental Science* 4 (2011) 2922–2929.
- [32] D. Lin-Vien, N. B. Colthup, W. G. Fatelley, J. G. Grasselli, *Academic Press Inc. San Diego*, 1991, pp 299–301.
- [33] J. Zhang, M.J. Li, Z.C. Feng, J. Chen, C. Li, *Journal of Physical Chemistry B* 110 (2006) 927–935.
- [34] F. Dong, L.W. Wu, Y.J. Sun, M. Fu, Z.B. Wu, S.C. Lee, *Journal of Materials Chemistry* 21 (2011) 15171–15174.
- [35] S.C. Yan, S.B. Lv, Z.S. Li, Z.G. Zou, *Dalton Transactions* 39 (2010) 1488–1491.
- [36] X.X. Xu, G. Liu, C. Random, J.T.S. Irvine, *International Journal of Hydrogen Energy* 36 (2011) 13501–13507.
- [37] Y.Q. Sun, C. Li, Y.X. Xu, H. Bai, Z.Y. Yao, G.Q. Shi, *Chemical Communications* 46 (2010) 4740–4742.
- [38] X.J. Wang, W.Y. Yang, F.T. Li, Y.B. Xue, R.H. Liu, Y.J. Hao, *Industrial and Engineering Chemistry Research* 52 (2013) 17140–17150.
- [39] Y. Wang, C.X. Feng, M. Zhang, J.J. Yang, Z.J. Zhang, *Applied Catalysis B: Environmental* 100 (2010) 84–90.
- [40] G.G. Zhang, J.S. Zhang, M.W. Zhang, X.C. Wang, *Journal of Materials Chemistry* 22 (2012) 8083–8091.
- [41] B. Chai, T.Y. Peng, J. Mao, K. Li, L. Zan, *Physical Chemistry Chemical Physics* 14 (2012) 16745–16752.
- [42] G.M. An, W.H. Ma, Z.Y. Sun, Z.M. Liu, B.X. Han, S.D. Miao, Z.J. Miao, K.L. Ding, *Carbon* 45 (2007) 1795–1801.
- [43] J.W. Ng, S.P. Xu, X.W. Zhang, H.Y. Yang, D.D. Sun, *Advanced Functional Materials* 20 (2010) 4287–4294.
- [44] I.H. Tseng, W.C. Chang, J.C.S. Wu, *Applied Catalysis B: Environmental* 37 (2002) 37–48.
- [45] G.H. Dong, L.Z. Zhang, *Journal of Materials Chemistry* 22 (2012) 1160–1166.
- [46] Q.G. Zhai, S.J. Xie, W.Q. Fan, Q.H. Zhang, W.P. Deng, Y. Wang, *Angewandte Chemie International Edition* 52 (2013) 5776–5779.